International Journal of Heat and Mass Transfer 52 (2009) 488–496

Contents lists available at ScienceDirect

International Journal of Heat and Mass Transfer

journal homepage: www.elsevier.com/locate/ijhmt

Methods of optimizing separation of compressible turbulent boundary-layer over a wedge with heat and mass transfer

M. Xenos [a], E. Tzirtzilakis [b], N. Kafoussias [b,*]

[a] University of Illinois at Chicago, Departments of Chemical Engineering and Bioengineering, Chicago 60607, IL, USA
[b] University of Patras, Department of Mathematics, Section of Applied Analysis, 26 500 Patras, Greece

ARTICLE INFO

Article history:
Received 15 December 2006
Received in revised form 10 April 2008
Available online 28 July 2008

Keywords:
Wedge flow
Compressible flow
Turbulent boundary-layer
Suction/injection

ABSTRACT

The steady, compressible, turbulent boundary-layer flow, with heat and mass transfer, over a wedge, is numerically studied. The fluid is considered to be a Newtonian ideal gas (air) and it is subject to a constant velocity of suction/injection applied globally or locally to the wedge.

The Reynolds-Averaged Boundary-Layer (RABL) equations and their boundary conditions are transformed using the compressible Falkner–Skan transformation. The resulting coupled and nonlinear system of PDEs is solved using the Keller-box method. For the eddy-kinematic viscosity the Cebeci–Smith and Baldwin–Lomax turbulent models are employed. For the turbulent Prandtl number the extended model of Kays–Crawford is used.

Numerical calculations are carried out for the case of an adiabatic, cooled or heated wall and for different values of the parameters of the problem under consideration. The obtained results show that the flow field can be controlled by the suction/injection velocity and it is influenced by the dimensionless pressure parameter m.

1. Introduction

A common area of interest in the field of aerodynamics is the investigation of compressible two-dimensional steady turbulent flows. A characteristic flow configuration, which is of fundamental importance, is that of the flow over a wedge. This type of flow constitutes a general class of problems in fluid mechanics in which the free stream velocity is proportional to a power of the length coordinate measured from the stagnation point.

The two-dimensional incompressible wedge flow investigated, for the first time, in 1931 by Falkner and Skan [1] and since then, it has been studied by many authors. The most recent and representative research works, for this type of flow, were presented in [2–9].

Suction/injection has very often been used as an active aerodynamic flow control technique to prevent transition from laminar to turbulent flow as well as turbulent flow separation as far as the aerodynamics is concerned [10]. The combined influence of localized injection and localized suction retains the boundary-layer flow, reducing skin friction [11,12]. Many passive and active techniques have been developed for the prevention or delay of flow separation. Passive techniques are currently employed via blown flaps on the tip of the aircraft wings or leading edge extensions and strakes on the nose of the wings (slats) or via vortex generators on various points on the wings [13]. Another mean of boundary-layer control is by heating or cooling the wall [14].

The numerical investigation of the two-dimensional turbulent boundary-layer compressible flow, with an adverse pressure gradient and heat and mass transfer, over a finite smooth and permeable flat surface, was studied in [15]. It was found that the continuous suction/injection applied on the wall modulates the flow field and the separation point in adiabatic, heating and cooling flat plates. The localized suction/injection moves the separation point downstream, and the local skin friction coefficient is smaller than in the corresponding case of continuous suction. The effect of suction/injection is less evident as the free stream Mach number increases. It is also worth mentioning that the boundary-layer over the heating wall is more sensitive to separation that that of the adiabatic and cooling walls.

As far as it could be investigated, the compressible turbulent boundary-layer flow over a wedge has not been yet studied. Hence, the aim of this work is the investigation of the classical wedge flow problem from the aerodynamics point of view. Thus, in the present study, the compressible turbulent boundary-layer flow over a permeable wedge is numerically studied. The effects of localized suction, applied to the region of the separation point, are also examined. The boundary-layer flow is considered turbulent and two turbulent models are employed, those of Cebeci–Smith (C–S) and Baldwin–Lomax (B–L). From the analysis of the obtained

* Corresponding author.
E-mail address: nikaf@math.upatras.gr (N. Kafoussias).

0017-9310/$ - see front matter © 2008 Elsevier Ltd. All rights reserved.
doi:10.1016/j.ijheatmasstransfer.2008.06.004

results it is concluded that localized suction or injection influences the flow field and the separation point, rendering the above application a flow control technique.

2. Mathematical formulation

The steady, two-dimensional, compressible and turbulent boundary-layer flow over a permeable wedge is considered. The wedge is submerged in a heat-conducting perfect and Newtonian fluid (air), with density ρ and thermal conductivity k, flowing with velocity u_∞ towards the wedge (Fig. 1). The fluid on the wedge is subjected to suction or blowing through the entire surface or locally from slots on various locations on the surface of the wedge. The suction/injection velocity on the wedge surface is $v_w(x)$; whereas the temperature of the surface of the wedge is $T_w(x)$.

Under the above assumptions, the equations governing this type of flow are the Reynolds-Averaged Boundary-Layer (*RABL*) equations, which can be written in the orthogonal system of coordinates shown in Fig. 1, as follows [14,15].

Continuity equation

$$\frac{\partial}{\partial x}(\bar{\rho}\bar{u}+\overline{\rho' u'})+\frac{\partial}{\partial y}(\bar{\rho}\bar{v}+\overline{\rho' v'})=0, \tag{1}$$

x - Momentum equation

$$(\bar{\rho}\bar{u}+\overline{\rho' u'})\frac{\partial \bar{u}}{\partial x}+(\bar{\rho}\bar{v}+\overline{\rho' v'})\frac{\partial \bar{u}}{\partial y}=-\frac{\partial \bar{p}}{\partial x}+\frac{\partial}{\partial y}\left[\mu\frac{\partial \bar{u}}{\partial y}-(\bar{\rho}\overline{u'v'}+\overline{\rho' u' v'})\right], \tag{2}$$

y - Momentum equation

$$\frac{\partial \bar{p}}{\partial y}=0, \tag{3}$$

Total-enthalpy equation

$$\bar{\rho}\bar{u}\frac{\partial H}{\partial x}+(\bar{\rho}\bar{v}+\overline{\rho' v'})\frac{\partial H}{\partial y}=\frac{\partial}{\partial y}\left[k\frac{\partial \bar{T}}{\partial y}-c_p\bar{\rho}\overline{T'v'}-c_p\overline{\rho' T' v'}+\bar{u}\left(\mu\frac{\partial \bar{u}}{\partial y}-\bar{\rho}\overline{u'v'}-\overline{\rho' u' v'}\right)\right] \tag{4}$$

It is worth mentioning here that the total enthalpy H for a perfect gas is defined by the expression:

$$H=c_pT+\frac{1}{2}u^2 \tag{5}$$

In the above equations we have replaced the instantaneous "quantities" f (e.g. u, v, T, ρ) by the sum of their mean ($\bar{f}$) and fluctuating parts (f'), that is $f=\bar{f}+f'$.

It can be proved, by applying an order-of-magnitude analysis [14], that density fluctuations are generally small in practice, both in low-speed flows with high heat transfer and in high-speed adiabatic-wall flows. Thus, terms containing ρ' can be dropped from the mass, momentum and enthalpy equations for thin shear layers. Also, the term $\overline{\rho' u'}$ is negligible compared with $\bar{\rho}\bar{u}$ as long as $(\gamma-1)M^2$ is not an order of magnitude greater than unity; whereas the term $\overline{\rho' v'}$ cannot be neglected, compared with $\bar{\rho}\bar{v}$, in the continuity, momentum and total-enthalpy equations.

On the other hand, the y-momentum Eq. (3) shows that the pressure variation is governed by the free stream and the term $\frac{\partial \bar{p}}{\partial x}$ in the x-momentum equation can be substituted by

$$-\frac{\partial \bar{p}}{\partial x}=-\frac{d\bar{p}}{dx}=\rho_e u_e\frac{du_e}{dx}, \tag{6}$$

where the subscript, e, refers to the conditions at the edge of the boundary-layer.

Due to the parabolic nature of the above equations, boundary conditions must be provided on two sides of the solution domain in addition to the initial conditions at $x = x_0$. So, the boundary conditions of the problem under consideration are

$$\begin{aligned} &y=0: u=0, v=v_w(x), \quad H=H_w(x)=c_pT_w(x),\\ &y=\delta: u=u_e(x), \quad H=H_e(x)=T_e(x)+\frac{1}{2}u_e^2(x). \end{aligned} \tag{7}$$

In the above boundary conditions (7) δ is a distance sufficiently far away from the wall where the u velocity and the temperature T reach their free stream values $u_e(x)$ and $T_e(x)$.

On the other hand, $v_w(x)$ is the mass transfer velocity at the wall and for the case of an impermeable wall $v_w(x)$ is equal to zero, for the case of suction $v_w(x) < 0$; whereas for the case of injection $v_w(x) > 0$.

In the flow over the wedge the velocity at the edge of the boundary-layer can be written as in [2]

$$u_e=u_\infty x^m, \quad m=\frac{\beta}{2-\beta}\geqslant 0, \tag{8}$$

where u_∞ is the free stream velocity and β is the Hartree pressure-gradient parameter that corresponds to $\beta = \omega/\pi$ for a total angle ω of the wedge. Using the abbreviation $\overline{\rho v}$ for $\rho v+\bar{\rho}\bar{v}$ and omitting,

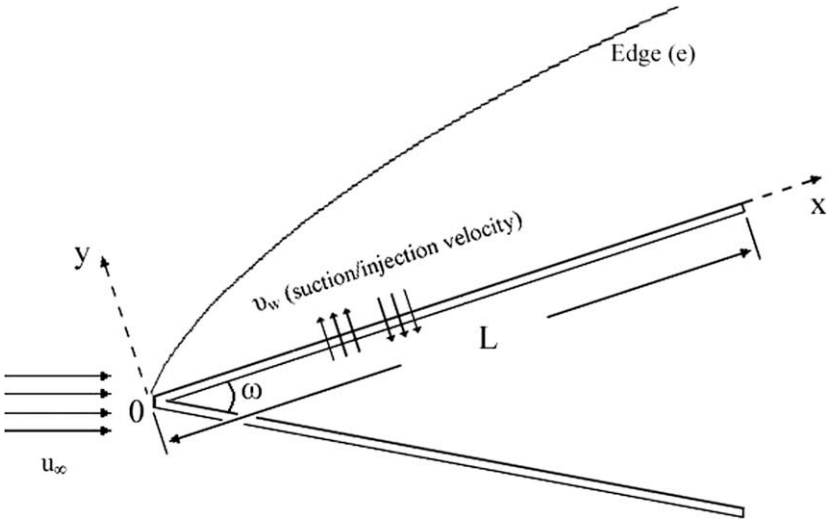

Fig. 1. Flow configuration and coordinate system for the wedge.

for simplicity, the over-bars on the basic time-average variables u, υ, ρ, p and T the equations of the problem can now be written as:

$$\frac{\partial}{\partial x}(\rho u)+\frac{\partial}{\partial y}(\overline{\rho\upsilon})=0, \tag{9}$$

$$\rho u\frac{\partial u}{\partial x}+\overline{\rho\upsilon}\frac{\partial u}{\partial y}=\rho_e u_e\frac{du_e}{dx}+\frac{\partial}{\partial y}\left[\mu\frac{\partial u}{\partial y}-\rho\overline{u'\upsilon'}\right], \tag{10}$$

$$\rho u\frac{\partial H}{\partial x}+\overline{\rho\upsilon}\frac{\partial H}{\partial y}=\frac{\partial}{\partial y}\left[k\frac{\partial T}{\partial y}-c_p\rho\overline{T'\upsilon'}+u\left(\mu\frac{\partial u}{\partial y}-\rho\overline{u'\upsilon'}\right)\right]. \tag{11}$$

Defining the eddy-kinematic viscosity ε_m and turbulent Prandtl number Pr_t by the expressions

$$-\overline{u'\upsilon'}=\varepsilon_m\frac{\partial u}{\partial y},\quad -\overline{T'\upsilon'}=\frac{\varepsilon_m}{Pr_t}\frac{\partial T}{\partial y}, \tag{12}$$

the equations describing the problem can be written as

$$\frac{\partial}{\partial x}(\rho u)+\frac{\partial}{\partial y}(\overline{\rho\upsilon})=0, \tag{13}$$

$$\rho u\frac{\partial u}{\partial x}+\overline{\rho\upsilon}\frac{\partial u}{\partial y}=\rho_e u_e\frac{du_e}{dx}+\frac{\partial}{\partial y}\left[(\mu+\rho\varepsilon_m)\frac{\partial u}{\partial y}\right], \tag{14}$$

$$\rho u\frac{\partial H}{\partial x}+\overline{\rho\upsilon}\frac{\partial H}{\partial y}=\frac{\partial}{\partial y}\left\{\left(\frac{\mu}{Pr}+\rho\frac{\varepsilon_m}{Pr_t}\right)\frac{\partial H}{\partial y}+\left[\mu\left(1-\frac{1}{Pr}\right)+\rho\varepsilon_m\left(1-\frac{1}{Pr_t}\right)\right]u\frac{\partial u}{\partial y}\right\}, \tag{15}$$

whereas the boundary conditions remain unchanged, that is

$$\begin{aligned}&y=0: u=0,\ \upsilon=\upsilon_w(x),\ H=H_w(x),\\ &y=\delta: u=u_e(x),\ H=H_e(x).\end{aligned} \tag{16}$$

The above system of Eqs. (13)–(16) is a coupled and nonlinear system of partial differential equations (PDEs).

In order to solve the system of PDEs numerically, the compressible version of the *Falkner–Skan* transformation for a wedge is introduced, defined by

$$\begin{aligned}\eta(x,y)&=\int_0^y\left(\frac{m+1}{2}\frac{u_e(x)}{v_e(x)x}\right)^{1/2}\frac{\rho(x,y)}{\rho_e(x)}dy,\\ \psi(x,y)&=\left(\frac{2}{m+1}\rho_e\mu_e u_e x\right)^{1/2}f(x,\eta),\end{aligned} \tag{17}$$

where $f(x,y)$ is the dimensionless stream function. Using the definition of the stream function ψ, for a two-dimensional compressible flow, that satisfies the continuity Eq. (13), with the relations

$$\rho u=\frac{\partial\psi}{\partial y},\quad \overline{\rho\upsilon}=-\frac{\partial\psi}{\partial x}, \tag{18}$$

and defining the dimensionless total energy ratio S as $S=H/H_e$, the system of the PDEs (13)–(16) finally becomes

$$(bf'')'+m_1ff''+m_2[c-(f')^2]=x\left[f'\frac{\partial f'}{\partial x}-f''\frac{\partial f}{\partial x}\right], \tag{19}$$

$$(eS'+df'f'')'+m_1fS'=x\left[f'\frac{\partial S}{\partial x}-S'\frac{\partial f}{\partial x}\right], \tag{20}$$

$$\begin{aligned}&\eta=0: f'=0,\ S=S_w(x,0),\\ &f_w(x)=f(x,0)=-\left(\frac{m+1}{2u_e\mu_e\rho_e x}\right)^{1/2}\int_0^x\rho_w(x,0)\upsilon_w(x)dx,\\ &\eta=\eta_e: f'=1,\ S=1,\end{aligned} \tag{21}$$

where η_e is the dimensionless thickness of the boundary-layer and primes denote partial differentiation with respect to η. The quantities b, C, c, d, e, m_1, m_2, ε_m^+ and R_x are defined as follows:

$$\begin{aligned}&b=C(1+\varepsilon_m^+),\quad C=\frac{m+1}{2}\frac{\rho(x,\eta)\mu(x,\eta)}{\rho_e(x)\mu_e(x)},\quad c=\frac{\rho_e(x)}{\rho(x,\eta)},\\ &d=\frac{Cu_e^2(x)}{H_e(x)}\left[1-\frac{1}{Pr}+\varepsilon_m^+\left(1-\frac{1}{Pr_t}\right)\right],\quad \varepsilon_m^+=\frac{\varepsilon_m}{\nu(x,\eta)},\\ &e=\frac{C}{Pr}\left(1+\varepsilon_m^+\frac{Pr}{Pr_t}\right),\quad m_2=\frac{x}{u_e(x)}\frac{du_e(x)}{dx},\quad R_x=\frac{u_e(x)x}{\nu_e(x)},\\ &m_1=\frac{1}{2}\left[1+m_2+\frac{x}{\rho_e(x)\mu_e(x)}\frac{d}{dx}(\rho_e\mu_e)\right].\end{aligned} \tag{22}$$

The problem under consideration is described by the system of Eqs. (19) and (20), subjected to the boundary conditions (21); whereas the coefficients entering into the equations are defined by the expressions (22).

3. Turbulence models

In this study two algebraic turbulence models, *Cebeci-Smith* (C–S) and *Baldwin–Lomax* (B–L), are used for the calculation of the eddy–viscosity, ε_m and a model for the turbulent–Prandtl number, Pr_t.

The C–S model [14,16,17] is one of the simplest turbulence models and its accuracy has been explored for a wide range of experimental data. It is a "Zero–equation PDE model", using only PDEs for the velocity field [18]. It has been used for a wide range of engineering problems providing accurate results [15,19]. The C–S turbulent model is a two-layer algebraic eddy viscosity model where the turbulent boundary-layer is treated as a composite layer consisting of inner and outer regions with separate expressions for the eddy-kinematic viscosity in each region. For the inner region (viscous sublayer) the *Prandtl–Van Driest* formulation is used while for the outer region the *Clauser* formulation is used [14].

Baldwin and Lomax improved the C–S turbulent model avoiding the necessity for finding the edge of the boundary-layer. B–L is an algebraic turbulent model that also treats the turbulent boundary-layer as a composite layer consisting of inner and outer regions. For the inner region the *Prandtl–Van Driest* formulation is used. For the outer region, Baldwin and Lomax introduced a new formulation according to which the product $y_{MAX}F_{MAX}$ replaces $\delta^* u_e$ in the *Clauser* formulation of the C–S model and the combination $y_{MAX}U_{DIF}^2/F_{MAX}$ replaces δU_{DIF} in the wake formulation [20].

The B–L turbulence model was developed for use in multi-dimensional Navier–Stokes machine codes [21,22] and the results from this model are in a good agreement with experimental data. Many researchers have adopted the B–L algebraic model for its simplicity, although modifications to its basic form have been employed [23]. To investigate the mass transfer through the surface of the wedge, in the B–L model, a formula for the suction/injection velocity is adopted. In this study the "damping–length" parameter A^+ is not considered constant, but as a function of the local density and viscosity values [14]. Finally, for the turbulent–Prandtl number Pr_t a modification of the extended *Kays and Crawford's* model is used [12,24].

4. Numerical solution

The numerical scheme used to solve the parabolic system of PDEs (19)–(22) is a version of the *Keller-box* method [14–16,25]. The scheme is unconditionally stable, and second-order accuracy is achieved with arbitrary x and η-spacing [26]. The governing equations are written as a first-order system and derivatives of the unknown functions $f(x,\eta)$, $S(x,\eta)$ with respect to η are introduced as new functions. Using central-difference derivatives for the unknown functions at the midpoints of the net rectangle, the resulting difference equations are implicit and nonlinear. The box-differencing scheme with Newton linearization is then applied to the first-order PDEs, giving rise to a block tridiagonal system, which is solved by the block elimination method [27].

For the dimensionless total enthalpy ratio S_w, on the surface of the wedge, three different cases are considered. The case $S'_w = 0$, describing no heat transfer between the wedge and the fluid (adiabatic flow) and the cases $S_w > 1$ and $S_w < 1$. For the heating/cooling of the wedge (wall) the dimensionless heat transfer parameter is considered $S_w > 1$, ($S_w = 2$) and $S_w < 1$, ($S_w = 0.25$), respectively. For determining the specific heat under constant pressure c_p, the Prandtl number Pr and the density ρ of the fluid (air) for temperatures varying from 100 to 2500 K, an interpolation formula is used. The data for the c_p, Pr and ρ were taken from tables [14,28]. The values of each quantity, for every value of temperature, are calculated by the successive linear interpolation approach known as Neville's algorithm [29].

The developed numerical code was examined for grid independency in a previous publication [30]. That study showed that a computational grid of 801×61 is sufficient to provide accurate numerical results by comparing the separation point, total drag and the maximum temperature for different grid realizations. The numerical implementation provides similar results for computations above 801×61 grid points and is not influenced by the increase of the Mach number [30]. However, in this study a grid of 1601×81 grid points was used, where 81 points were used on the η-direction and 1601 on the x-direction. The length (L) of the wedge was taken for all calculations up to 8 m.

For the numerical solution of the equations describing the problem the program is divided in two parts. The first is a dynamic link library (*DLL*) which contains all the algorithms for the numerical solution of the problem. The second part is a graphical user interface (*GUI*), where the user can review or alter the initial data, as, for instance, the free stream Mach number, the temperature of the plate and the fluid, the suction/injection velocity, etc. The program was written in *FORTRAN 90* utilizing *OpenGL* for the visualization of the data [31].

5. Results and discussion

The results of this study concern dimensionless as well as dimensional quantities of the compressible turbulent boundary-layer over the wedge. It is very important to present results on the dimensionless local skin friction coefficient, C_{fx} and the local Stanton number, St_x, for heated and cooled walls, as well as the total drag D, over the wedge. It is also imperative to present results for dimensional quantities that will provide information for the shape of the compressible turbulent boundary-layer under the adverse pressure gradient, e.g. the velocity and temperature fields throughout the boundary-layer.

Fig. 2a presents the velocity field on the upper wall of a wedge for $m = 0.1$, ($\omega = 32.7°$) and $m = 0.2$, ($\omega = 60°$). The boundary-layer is always attached to the plate and never separates from the surface for Mach number $M_\infty = 0.75$. The figure also depicts the temperature field over the upper surface of the wedge for adiabatic wall (Fig. 2b, $S'_w = 0$), heated (Fig. 2c, $S_w = 2.0$) and cooled wall (Fig. 2d, $S_w = 0.25$) for both cases ($m = 0.1$ and 0.2). The increase of temperature in the boundary-layer for the adiabatic case is 6.5 degrees for $m = 0.1$ and 10.3 degrees for $m = 0.2$. This temperature increase is due to viscous forces acting on the flow field and the inclination of the wall. The maximum temperature for the adiabatic case is 306.5 K for $m = 0.1$ and 310.3 K for $m = 0.2$, for the heated wall is 410.3 K for $m = 0.1$ and 616.8 K for $m = 0.2$, and occurs near the heated wall. Finally, the maximum temperature for the cooled wall is 306.1 K for $m = 0.1$ and 310.1 K for $m = 0.2$, and occurs near the edge of the boundary-layer of the wedge as shown in Fig. 2d.

The flow over a flat plate at zero incidence, with constant external velocity, is known as *Blasius* flow and corresponds to the dimensionless pressure gradient $m = 0$. The dimensionless parameter m plays an important role in this type of problem because it denotes the shape factor of the velocity profiles [2]. It has been shown that when $m < 0$ (increasing pressure), the velocity profiles have a point of inflexion; whereas when $m > 0$ (decreasing pressure), there is no point of inflexion for the laminar boundary-layer [16]. In the case under consideration (steady, two-dimensional, compressible and turbulent boundary-layer flow) the investigation is limited only for $m \geqslant 0$ and results are presented for these values of m. In order to quantify the boundary-layer over a wedge, important dimensionless quantities, like the dimensionless local skin friction coefficient C_{fx}, the local Stanton number St_x and the total drag D, over the wedge, are presented. Eq. (23), shows the relationship that connects these quantities with the dimensionless shear parameter on the wall $f''_w = f''(x,0)$, the dimensionless heat transfer parameter $S'_w = S'(x,0)$ and the dimensionless total enthalpy ratio $S_w = H_w/H_e$ on the wall of the wedge [15,25].

$$C_{fx} = \left(\frac{m+1}{2}\right)^{1/2} \frac{2C_w}{\sqrt{R_x}} f''_w, \quad St_x = \left(\frac{m+1}{2}\right)^{1/2} \frac{C_w S'_w}{Pr\sqrt{R_x}(1-S_w)}, \quad (S_w \neq 1), \tag{23}$$

$$D = 2\left(\frac{m+1}{2}\right)^{1/2} \int_0^{x^*} \frac{C_w f''_w(x,0)}{\sqrt{\mathrm{Re}_x}} \rho_e(x) u_e^2(x)\,\mathrm{d}x$$

In the above expression, x^* is the distance of the separation point from the leading edge and $C_w = \rho_w\mu_w/\rho_e\mu_e$. Also, the total drag D is evaluated for both walls of the two-dimensional wedge. Fig. 3 shows the skin friction coefficient C_{fx}, against the distance x for various values of the parameter m ($m = 0.0, 0.2, 0.4, 0.6, 0.8$), for $M_\infty = 0.75$ and for the two turbulence models (C–S, B–L) for the case of an adiabatic wall. For small values of the dimensionless parameter m ($m \leqslant 0.6$), no separation occurs of the compressible turbulent boundary-layer over the wedge for the whole length of $8.0m$. For larger values of the dimensionless parameter m ($m > 0.6$), the model predicts separation of the turbulent compressible boundary-layer. Both turbulent models give similar results and as the angle of the wedge is increased the total drag D, and the skin friction coefficient C_{fx}, increase in both C–S and B–L models. In the case that $m = 0.8$, the separation of the compressible turbulent boundary-layer occurs at $x^* = 3.84m$ for the C–S and at $x^* = 4.16m$ for the B–L turbulence model.

The same behavior is shown for smaller ($M_\infty = 0.5$) or larger ($M_\infty = 1.25$) Mach numbers. The results for the total drag D, for various Mach numbers M_∞, for both turbulent models and for $m = 0.0, 0.1, 0.2$ and for an adiabatic wall are summarized in Table 1.

The results for heated and cooled walls of the wedge are similar with those of the adiabatic case. Figs. 4 and 5, depict the skin friction coefficient C_{fx}, against the distance x, for the cases of cooled and heated wedge walls, respectively, and for the various values of the dimensionless pressure parameter m ($m = 0.0, 0.2, 0.4, 0.6, 0.8$). The figures show that separation occurs only when $m > 0.6$ for both turbulence models and for both cases (heated and cooled walls). For $m = 0.8$ the separation point for the cooled wall is at $x^* = 4.51m$ for the C–S model and at $x^* = 4.66m$ for B–L. On the other hand, for $m = 0.8$ and heated, wall the predicted separation point for the C–S model is at $x^* = 3.39m$ and at $x^* = 3.77m$ for the B–L turbulence model. In all cases examined until now, the total drag D, increases as the dimensional pressure parameter m increases, and as a first result, can be concluded that the increase of parameter m, increases the skin friction coefficient C_{fx} and the total drag D, over the wedge.

One of the control methods that can retain the turbulent compressible boundary-layer over the wedge for larger values of the dimensionless pressure parameter m is the application of

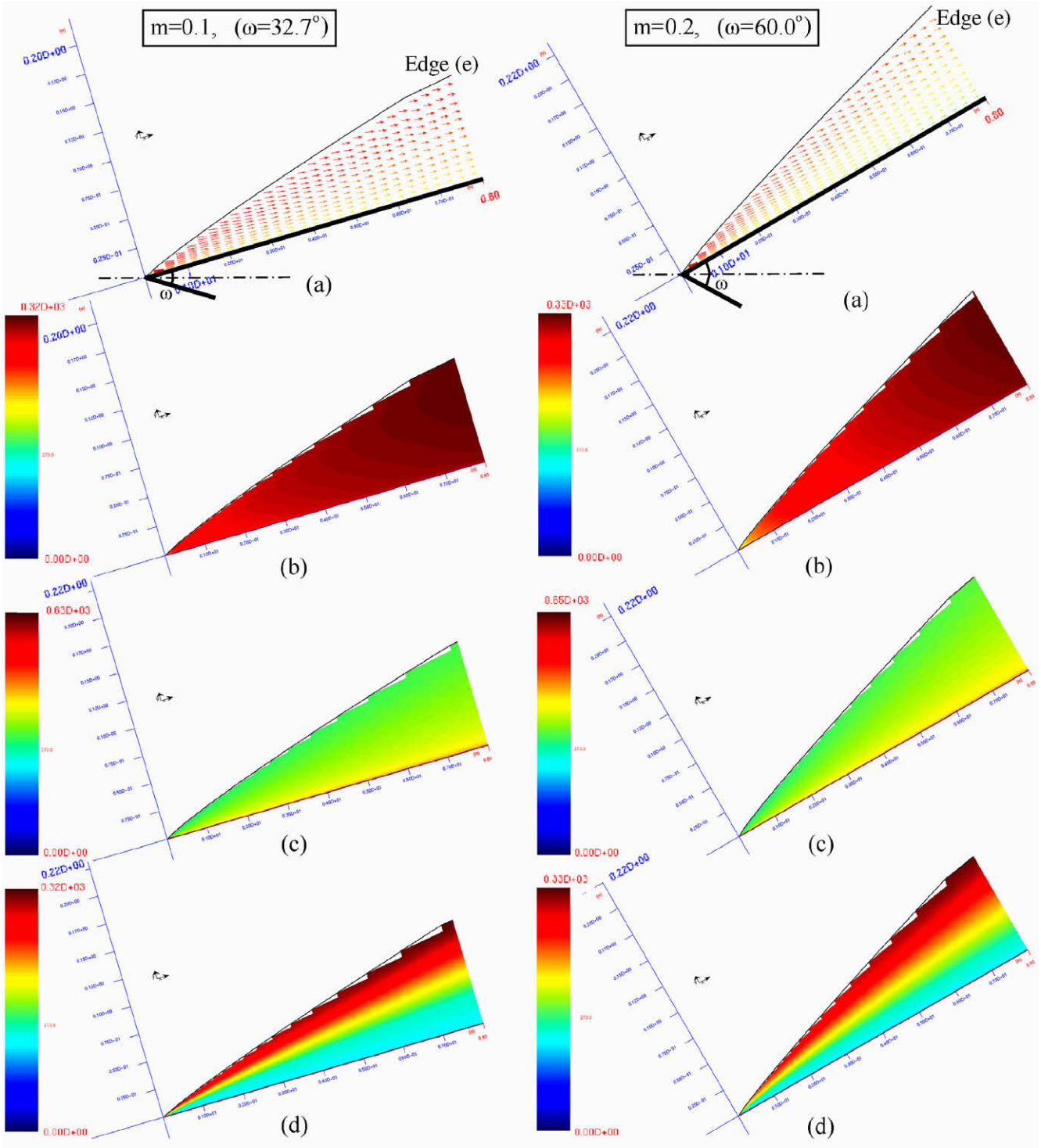

Fig. 2. (a) Velocity field over a wedge for $m = 0.1$ – left and $m = 0.2$ – right, (b) temperature field for an adiabatic wall for $m = 0.1$ – left and $m = 0.2$ – right, (c) temperature field for a heated wall for $m = 0.1$ – left and $m = 0.2$ – right, (d) temperature field for a cooled wall for $m = 0.1$ – left and $m = 0.2$ – right. $M_\infty = 0.75$.

continuous or localized suction/injection. Fig. 6 shows the skin friction coefficient C_{fx}, against the distance x, for $m = 0.2$ and 0.8 with or without suction/injection and for $M_\infty = 1.25$. The application of suction is continuous at the whole length of the upper wall of the wedge ($v_w(x) = -2.0 \times 10^{-4}$) or localized near the tip of the wedge ($v_w(x) = -6.0 \times 10^{-4}$). The left part of Fig. 6 shows the influence of localized and continuous suction when m is small ($m = 0.2$). The compressible turbulent boundary-layer is retained on the wall for this case and separation does not occur at the whole length of the adiabatic plate. The application of continuous suction increases the total drag but the localized suction has a smaller effect on D. The right part of Fig. 6, reveals the influence of suction when m is large ($m = 0.8$). In this case, the application of continuous suction moves the separation point downstream and retains the boundary-layer on the adiabatic wall of the wedge. So, at $m = 0.8$ with no suction or injection the separation point is at $x^* = 4.02m$, but after continuous suction the separation occurs at $x^* = 4.19m$. The localized suction applied at the tip of the wedge

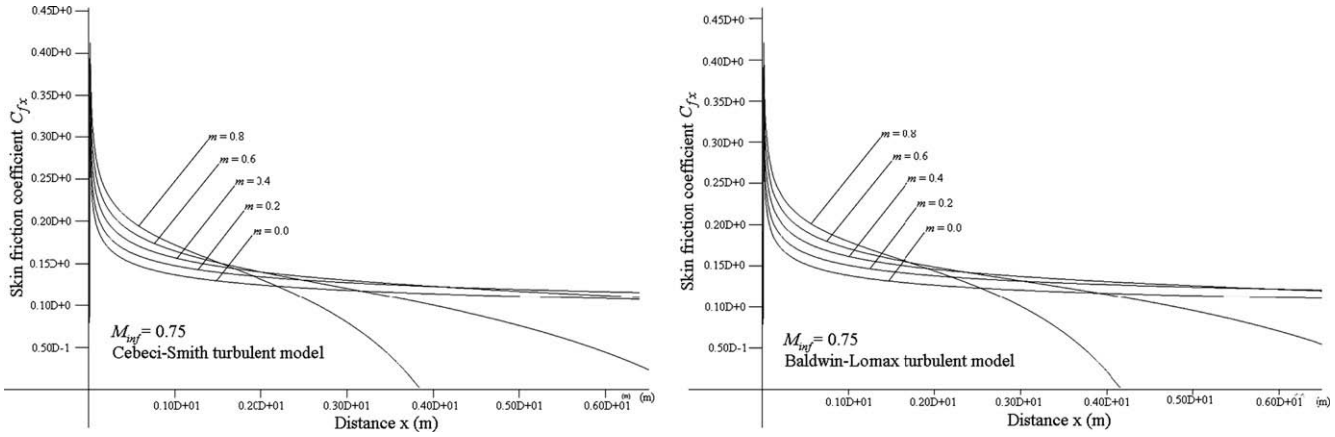

Fig. 3. Skin friction coefficient C_{fx}, against the distance x, for various values of the parameter m, for $M_\infty = 0.75$ and for the case of an adiabatic wall (C–S – left, B–L – right).

Table 1
Total drag D for various Mach numbers M_∞ and dimensionless pressure parameter m for an adiabatic wall

	C–S model		B–L model	
$M_\infty = 0.5$	$m = 0.0$	$D = 355.25$	$m = 0.0$	$D = 362.32$
	$m = 0.1$	$D = 362.47$	$m = 0.1$	$D = 371.58$
	$m = 0.2$	$D = 363.72$	$m = 0.2$	$D = 375.21$
$M_\infty = 0.75$	$m = 0.0$	$D = 749.52$	$m = 0.0$	$D = 767.03$
	$m = 0.1$	$D = 771.22$	$m = 0.1$	$D = 793.61$
	$m = 0.2$	$D = 780.98$	$m = 0.2$	$D = 809.16$
$M_\infty = 1.25$	$m = 0.0$	$D = 1891.14$	$m = 0.0$	$D = 1947.16$
	$m = 0.1$	$D = 1997.23$	$m = 0.1$	$D = 2070.94$
	$m = 0.2$	$D = 2081.80$	$m = 0.2$	$D = 2176.54$

has the same effect as the continuous suction shifting the separation point downstream at $x^* = 4.14m$. The total drag in the case of localized suction is smaller than that in the case of continuous, as shown in Fig. 6.

Similar results are observed in the cases of heated and cooled wedge walls. These results are illustrated in Figs. 7 and 8, respectively, for two different dimensionless pressure parameters ($m = 0.2$ and 0.8). In both cases (heated and cooled wedge walls) continuous and localized suction increases total drag but in the case of $m = 0.2$ they retain the compressible turbulent boundary-layer and prevent separation. The applied localized suction, near the tip of the wedge, was $\upsilon_w(x) = -4.0 \times 10^{-4}$ and the continuous suction, at the whole length of the upper wall of the wedge, was $\upsilon_w(x) = -1.5 \times 10^{-4}$ for the case of a heated wall. On the other hand, the applied localized suction, near the tip of the wedge, was $\upsilon_w(x) = -5.0 \times 10^{-4}$ and the continuous suction, at the whole length of the upper wall of the wedge, was $\upsilon_w(x) = -2.0 \times 10^{-4}$ for the case of a cooled wall. More precisely, in Fig. 7 right, separation occurs at $x^* = 3.59m$ with the application of continuous suction and at $x^* = 3.67m$ with the application of localized, in respect to the initial case (no suction/injection) that separation occurs at $x^* = 3.63m$. In Fig. 8 right, separation occurs at $x^* = 4.56m$ for continuous suction and at $x^* = 4.68m$ for localized, in respect to the initial case (no suction/injection) where separation occurs at $x^* = 4.64m$. It is apparent that the compressible turbulent boundary-layer can be retained with the application of suction, but the total drug D, increases especially in the case of continuous suction as shown in the figures.

In Fig. 9, the local Stanton number St_x is presented, for heated and cooled walls and different values of the dimensionless pressure parameter m ($m = 0.0, 0.2, 0.4, 0.6, 0.8$), for the C–S turbulence model. So, at each case (heated and cooled walls) the local Stanton number St_x, increases as the parameter m increases and this is due to the friction effects on the wall of the wedge that are more pronounced when the inclination of the wedge increases. Fig. 10, depicts the influence of continuous and localized suction on the local Stanton number. The dimensionless pressure parameter m, was chosen equal to 0.8 and the turbulence model used for these simulations is the C–S. The case of $m = 0.0$ is also presented for comparison with the cases of $m = 0.8$ no suction/injection, continuous and localized suction. The continuous as well as the localized suction increases the local Stanton number St_x, over the wedge in

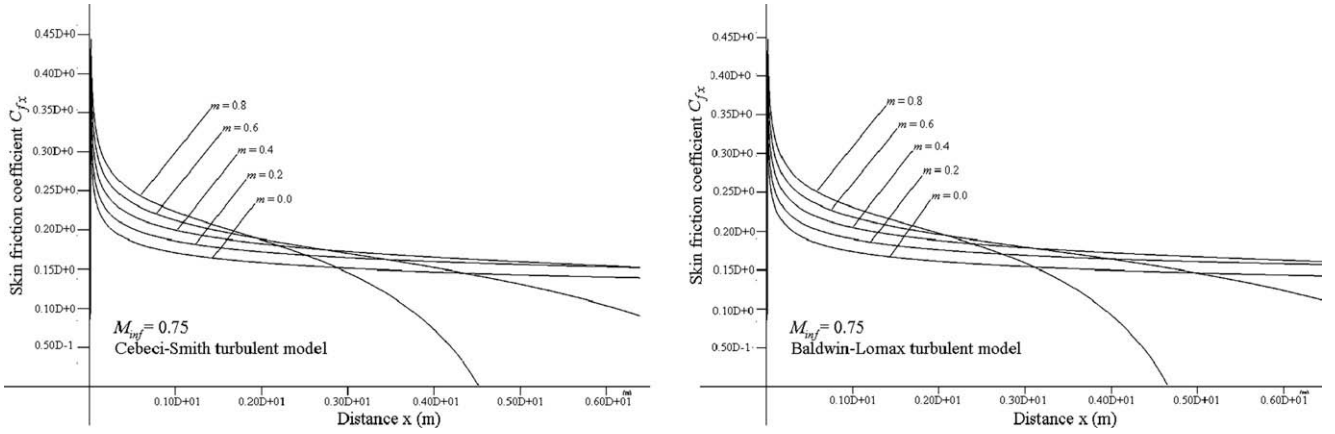

Fig. 4. Skin friction coefficient C_{fx} against the distance $x$for various values of the parameter m, for $M_\infty = 0.75$ and for the case of a cooling wall (C–S – left, B–L – right).

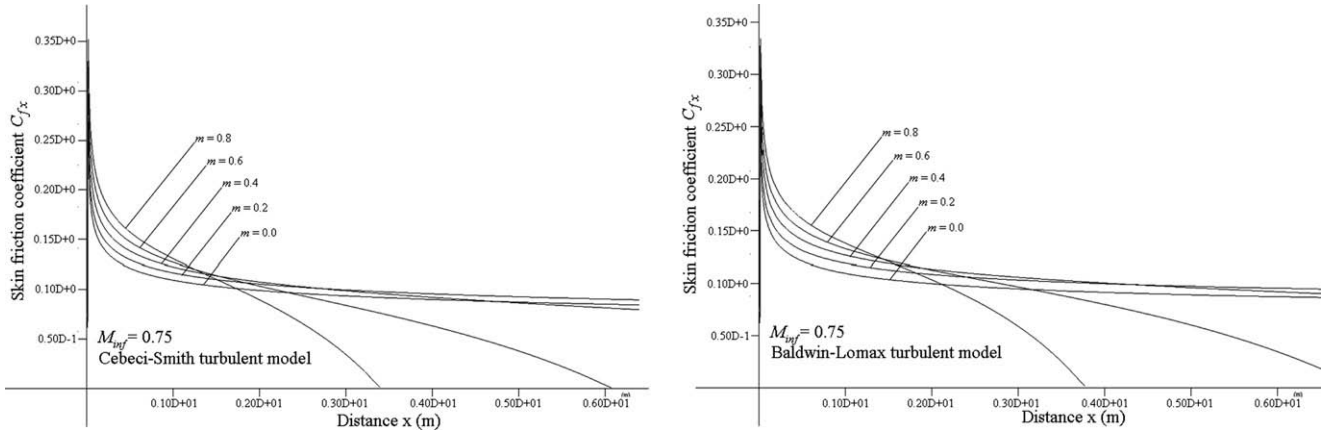

Fig. 5. Skin friction coefficient C_{fx} against the distance x for various values of the parameter m, for $M_\infty = 0.75$ and for the case of a heated wall (C–S – left, B–L – right).

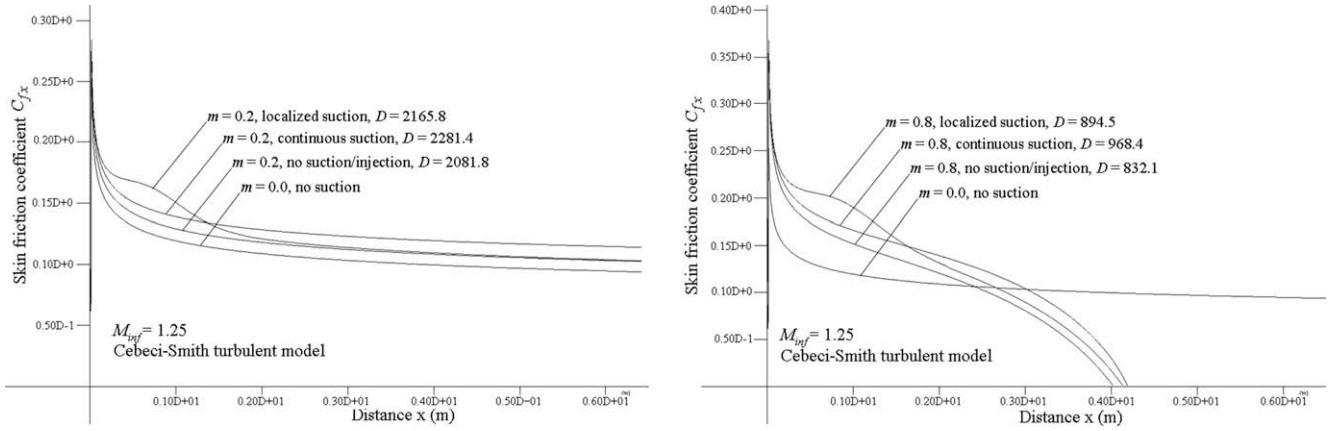

Fig. 6. Skin friction coefficient C_{fx}, against the distance x, for various values of the parameter m ($m = 0.2$ and 0.8), for $M_\infty = 1.25$ and for the case of an adiabatic wall and application of continuous and localized suction (C–S turbulent model).

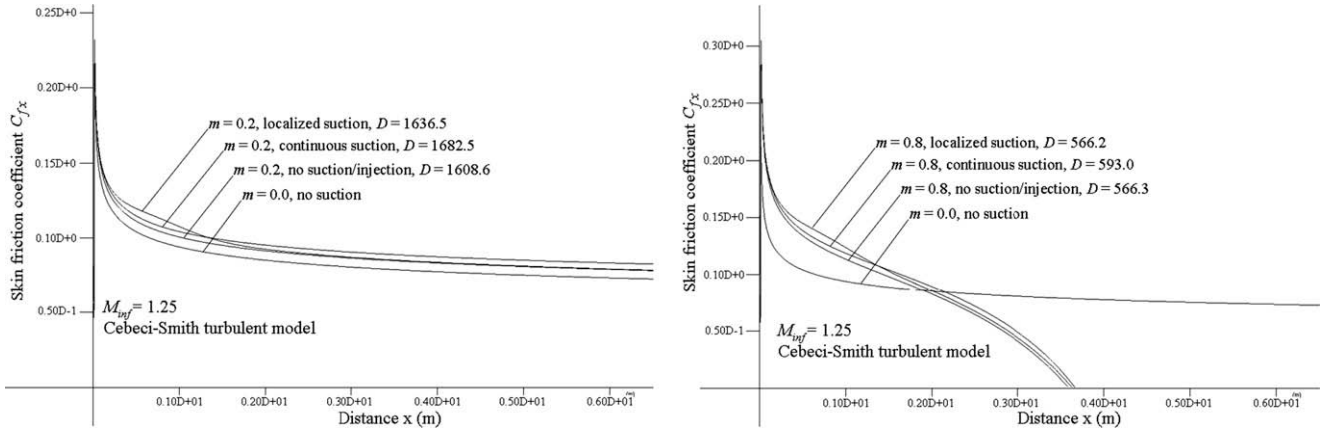

Fig. 7. Skin friction coefficient C_{fx}, against the distance x, for various values of the parameter m ($m = 0.2$ and 0.8), for $M_\infty = 1.25$ and for the case of a heated wall and application of continuous and localized suction (C–S turbulent model).

both cases of Fig. 10 (heated and cooled walls) and this increase is more evident in the case of cooled walls.

Finally, in an effort to describe the variation of the total drag D, with respect to the Mach number $M_\infty = M_{\text{inf}}$, Fig. 11 presents the variation of D, against M_∞, for a small dimensionless pressure parameter m ($m = 0.1$) and for an adiabatic wedge wall. The cases of no suction/injection, continuous suction at the whole length of the wedge ($8.0m$) and continuous injection are presented. For the whole range of Mach numbers investigated ($M_\infty = 0.25$ until 2.25 *Mach*) the total drag D, is always larger in the case of continuous suction as expected. The total drag is always smaller in the case of continuous injection in respect to the cases of no suction/injection and continuous suction. So, a combination of localized suction and localized injection would be the most beneficial tradeoff and is widely used in our days in all modern airplanes, for drag reduction and boundary-layer prevention of separation especially during takeoff and landing.

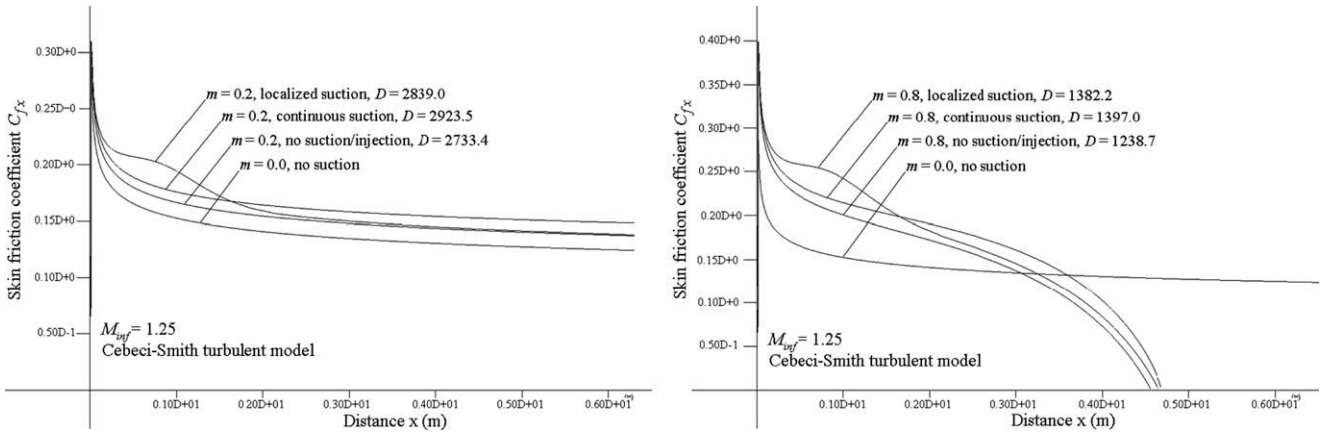

Fig. 8. Skin friction coefficient C_{fx}, against the distance x, for various values of the parameter m (m = 0.2 and 0.8), for M_∞ = 1.25 and for the case of a cooled wall with application of continuous and localized suction (C–S turbulent model).

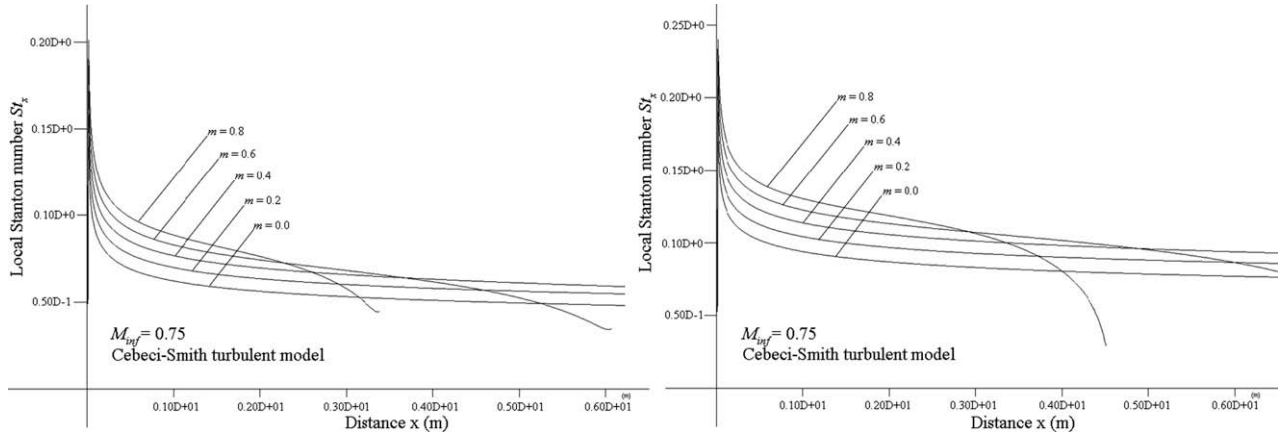

Fig. 9. Local Stanton number St_x, for heated – left and cooled – right walls and different values of the dimensionless pressure parameter m (C–S turbulent model).

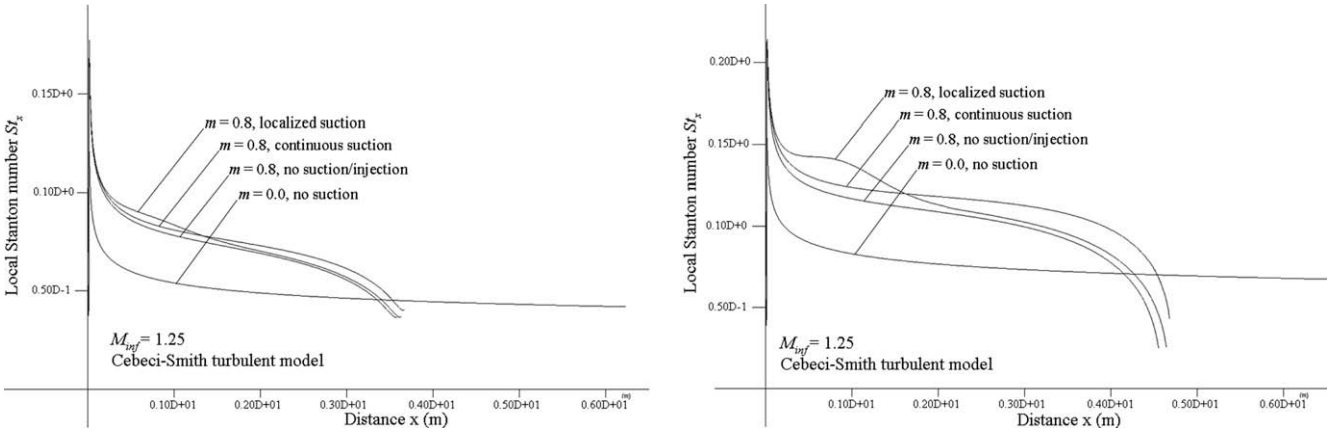

Fig. 10. Local Stanton number St_x for heated – left and cooled – right walls and different values of the dimensionless pressure parameter m (C–S turbulent model) with suction/injection.

6. Conclusions

- A mathematical formulation for the turbulent compressible boundary-layer flow over a wedge was presented.
- Different values of the dimensionless pressure parameter m were examined (m = 0.0, 0.2, 0.4, 0.6, 0.8). When m increases, the dimensionless skin friction coefficient C_{fx}, the local Stanton number St_x, and the total drag D, increase as shown in the figures.

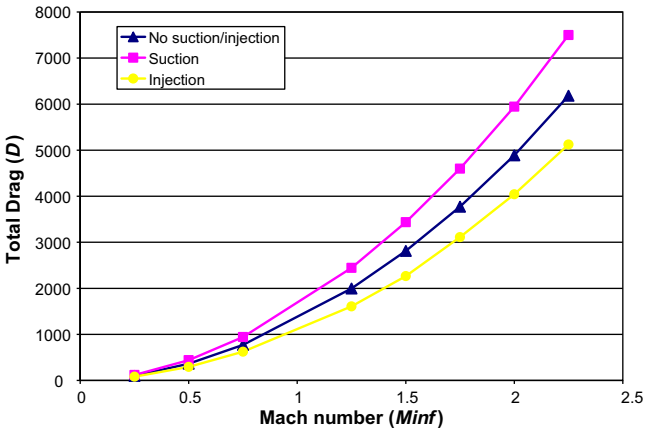

Fig. 11. Total drag D with respect to the Mach number for the cases of no suction/injection, suction and injection, for a specific inclination of an adiabatic wedge ($m = 0.1$).

- Small values of m ($m \leqslant 0.6$), does not lead to boundary-layer separation in the 8m length of the wedge wall. Though, increasing m ($m > 0.6$), separation occurs for all cases of adiabatic, cooled and heated walls of the wedge.
- Application of continuous suction retains the boundary-layer downstream to the flow but increases total drag. Localized suction retains the boundary-layer downstream to the flow and is more desirable due to smaller total drag D, than the continuous suction case.
- Suction always increases the total drag over the wedge. On the other hand, injection decreases the total drag over the wedge and the combination of the localized suction and injection is important for drag reduction and prevention of boundary-layer separation.

Acknowledgments

The authors want to thank *S. Dimas* for his contribution to the construction of the *GUI* of this code. The authors also thank the *European Social Fund* (*ESF*), Operational Program for Educational and Vocational Training II (*EPEAEK II*), and particularly, the Program PYTHAGORAS II, for funding the present study.

References

[1] V.M. Falkner, S.W. Skan, Some approximate solutions of the boundary layer equations, Philos. Mag. 12 (80) (1931) 865–896.
[2] N.G. Kafoussias, N.D. Nanousis, Magnetohydrodynamic laminar boundary-layer flow over a wedge with suction or injection, Can. J. Phys. 75 (1997) 733–745.
[3] M.A. Hossain, M.S. Munir, D.A.S. Rees, Flow of viscous incompressible fluid with temperature dependent viscosity and thermal conductivity past a permeable wedge with uniform surface heat flux, Intl. J. Therm. Sci. 39 (2000) 635–644.
[4] M. Massoudi, Local non-similarity solutions for the flow of a non-Newtonian fluid over a wedge, Intl. J. Non-Linear Mech. 36 (2001) 961–976.
[5] W.T. Cheng, H.T. Lin, Non-similarity solution and correlation of transient heat transfer in laminar boundary layer flow over a wedge, Intl. J. Eng. Sci. 40 (2002) 531–548.
[6] S.P.A. Devi, R. Kandasamy, Thermal stratification effects on non linear MHD laminar boundary-layer flow over a wedge with suction or injection, Intl. Commun. Heat Mass Trans. 30 (5) (2003) 717–725.
[7] K. Bor-Lih, Heat transfer analysis for the Falkner–Skan wedge flow by the differential transformation method, Intl. J. Heat Mass Trans. 48 (2005) 5036–5046.
[8] R. Kandasamy, K. Periasamy, K.K. Sivagnana Prabhu, Effects of chemical reaction, heat and mass transfer along a wedge with heat source and concentration in the presence of suction or injection, Intl. J. Heat Mass Trans. 48 (2005) 1388–1394.
[9] A. Pantokratoras, The Falkner–Skan flow with constant wall temperature and variable viscosity, Intl. J. Therm. Sci. 45 (2006) 378–389.
[10] D. Arnal, Control of laminar–turbulent transition for skin friction drag reduction, in: Control of Flow Instabilities and Unsteady Flows, CISM Course, September 18–22, 1995, pp. 119–153.
[11] S. Roy, Nonuniform slot injection (suction) into a compressible flow, Acta Mechanica 139 (2000) 43–56.
[12] M. Xenos, N. Kafoussias, G. Karahalios, Magnetohydrodynamic compressible laminar boundary layer adiabatic flow with adverse pressure gradient and continuous or localized mass transfer, Can. J. Phys. 79 (2001) 1247–1263.
[13] M. Gad-el-Hak, D.M. Bushnell, Status and Outlook of Flow Separation Control, AIAA Paper 91-0037, 1991.
[14] T. Cebeci, P. Bradshaw, Physical and Computational Aspects of Convective Heat Transfer, Springer Verlag, New York, 1984. p. 174.
[15] N. Kafoussias, M. Xenos, Numerical investigation of two-dimensional turbulent boundary-layer compressible flow with adverse pressure gradient and heat and mass transfer, Acta Mechanica 141 (2000) 201–223.
[16] H. Schlichting, Boundary-Layer Theory, in: J. Kestin (Ed.), sixth ed., McGraw-Hill Inc., New York, 1968, p. 645 (Trans.).
[17] T. Cebeci, A.M.O. Smith, Analysis of Turbulent Boundary Layers, Academic Press, New York, 1974. pp. 329–370 and 258–296.
[18] P. Bradshaw (Ed.), Turbulence, Topics in Applied Physics, 12, Springer Verlag, Berlin, 1976, pp. 193–195.
[19] R.A.W.M. Henkes, Scaling of equilibrium boundary layers under adverse pressure gradient using turbulent models, AIAA J. 36 (3) (1998) 320–326.
[20] B. Baldwin, H. Lomax, Thin-Layer Approximation and Algebraic Model for Separated Turbulent Flows, AIAA Paper 78–205, 1978.
[21] J.L. Steger, Implicit finite difference simulation of flow about arbitrary geometries with application to airfoils, AIAA Paper 77–665, Presented at AIAA 12th Thermo Physics Conference at Albuquerque, New Mex., June 27–29, 1977.
[22] T.H. Pulliam, J.L. Steger, Implicit finite-difference simulations of three-dimensional compressible flow, AIAA J. 18 (2) (1980) 159–167.
[23] C.J. Tam, P.D. Orkwis, Comparison of Baldwin–Lomax turbulence models for two-dimensional open cavity computations, AIAA J. 34 (3) (1995) 629–631.
[24] B. Weigand, J. R Ferguson, M.E. Crawford, An extended Kays and Crawford turbulent Prandtl number model, Intl. J. Heat Mass Trans. 40 (17) (1997) 4191–4196.
[25] N. Kafoussias, A. Karabis, M. Xenos, Numerical study of two dimensional laminar boundary layer compressible flow with pressure gradient and heat and mass transfer, Intl. J. Eng. Sci. 37 (1999) 1795–1812.
[26] H.B. Keller, A new difference scheme for parabolic problems, in: J. Bramble (Ed.), Numerical Solutions of Partial Differential Equations, II, Academic Press, New York, 1970.
[27] J.C. Tannehill, D.A. Anderson, R.H. Pletcher, Computational Fluid Mechanics and Heat Transfer, second ed., Taylor & Francis, London, 1997.
[28] J.H. Davidson, F.A. Kulacki, P.F. Dunn, Convective heat transfer with electric and magnetic fields, in: S. Kakac, R.K. Shah, W. Aung (Eds.), Handbook of Single-Phase Convective Heat Transfer, John Wiley & Sons, New York, 1987, pp. 9.1–9.49.
[29] W.A. Cecilio, C. J Cordeiro, I.S. Milleo, C.D. Santiago, R.A.D. Zanardini, J.Y. Yuan, A note on polynomial interpolation, Intl. J. Comput. Math. 79 (4) (2002) 465–471.
[30] M. Xenos, S. Dimas, N. Kafoussias, MHD compressible turbulent boundary layer flow with adverse pressure gradient, Acta Mechanica 177 (1–4) (2005) 171–190.
[31] R.S. Wright Jr., M.R. Sweet, OpenGL Super Bible, second ed., Waite Group Press, San Francisco, 1999.